Danish Meteorological Institute
Ministry of Transport and Energy

dmi.dk

Scientific Report 05-03

Application of Full Spectrum Inversion Techniques: Data processing methods and spatial accuracy

Copenhagen 2005

Colophon

Serial title:
Scientific Report

Title:
Application of Full Spectrum Inversion Techniques

Subtitle:
Data processing methods and spatial accuracy

Author(s):
Arne Skov Jensen, Christian Marquardt, Hans-Henrik Benzon, Martin .S. Lohmann

Other contributors:

Responsible institution:
DMI

Language:
English

Keywords:
Full Spectrum Inversion, FSI, Radio Occultations, Phasematching

Url:
www.dmi.dk/dmi/sr05-03

Digital ISBN:
87-7478-520-6

ISSN:
1399-1949 (online)

Version:

Website:
www.dmi.dk

Content:

Abstract

The *Full Spectrum Inversion* (FSI) method was developed in the start of 2002 in order to solve the multipath problem in radio occultation measurements. The physical ideas which lead to the method were that the occultation path could be considered as a synthetic aperture and the Radio occultation Doppler frequency in a single path was a monotonic function of time. In star occultation's, at optical wavelengths, the multipath problem is easily solved by having a lens in front of an array detector separating the beams in space. The lens is performing a spatial Fourier transform i.e. a plane wave is focused into a point displaced from the optical axis an amount given by the direction (the spatial frequency) of the plane wave. The analogy to this space processing method in time, is to have a 'time lens' which can separate multiple temporal frequencies occurring at the same time: Obviously this is what a temporal Fourier transform does. These ideas were implemented in 2001 and tested successfully on simulations of radio occultation signals with circular satellite path. However, for non-circular orbits the plain Fourier method turned out to give not a fully correct result and the work on the FSI emerged realizing that some preprocessing steps where necessary in order to eliminate the impact of non-radial orbits. This involves pre-calculation of phases which multiplied on the occultation signal reduces the impact of the non-circular orbits on the resulting Fourier transform of preprocessed signal. In 2003 the *Phasematching method* was developed where the impact of the non-circular orbits was totally solved, but with the cost that the processing could not be implemented with a fast Fourier transform.

In the FSI paper [Jensen et al, 2003] the practical implementation and the spatial resolution of the method was not addressed. General theoretical consideration about the spatial resolution was addressed in [Jensen et. al, 2002b]. In the present report on the development of the FSI method include its practical implementation making the method robust for mass processing of radio occultation signals. An element in the FSI method is an upsampling of the radio occultation signal. This has the result that the time of arrival of the rays apparently can be determined with accuracy equal to the upsampled time interval. This accuracy is however false and one must consider the time of arrivals of the rays as random in the original sampling time interval. The consequence of this is an intrinsic uncertainty in spatial resolution of the FSI method. A method for dealing with this is developed in this report. For the development of the practical implementation, so the method is robust and can be used for mass processing of radio occultation signals, noise discrimination of the outcome of the FSI method is important. A new method of discriminating noise in the differentiated phase of the Fourier transform has been developed and demonstrated in the report.

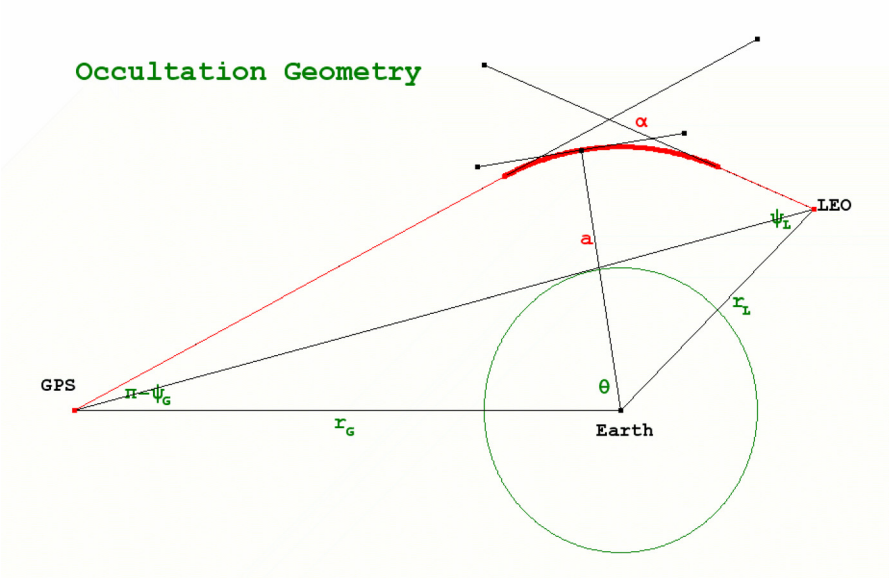

1. Introduction

A short overview of the basic physical and mathematical tools for a description of radio occultation signals is given in this part. Most of the formulas and theoretical description can be found in [Jensen et. al, 2003] and [Jensen et. al, 2004], though the presentation here hopefully represent a more pedagogical view. In sec. 2 the general phasematching scheme is described. In Sec.3.1 an implementation of the FSI method is shown and discussed. The present implementation of the FSI is the one used by the authors of this paper; other implantation schemes are surely possible. This is an ongoing development and research. In Sec. 3.2 a discrimination technique for time of arrival spectrum is introduced.

In Sec.3.3 a new method for filtering and a conversion of the time of arrival uncertainties to Doppler frequencies uncertainties is proposed. This part is important and gives estimates of the spatial resolution of the refractivity or the bending angle for an actual occultation signal. In Sec.3.4 the effect of thermal noise on the time of arrivals are calculated. The results of this is not used explicitly here but just noted for eventually future use.

1.1 The radio occultation signal

The received radio signal at the LEO satellite is a narrow banded signal with a carrier frequency determined by the transmitting GPS satellite. The electromagnetic field is formed by the refractive structure of the atmosphere. The GPS and the LEO satellite are moving during the occultation. The path of the LEO satellite can be considered as a synthetic aperture. In principle, the resulting field should be computed from Maxwell equations for an actual refractive structure. An analytical solution has not been found and it can probably not be done. Instead, a geometrical optical description is applied in order to analyze possible signal processing methods.

1.2 Geometrical optical description

The geometrical optical description implies a ray description instead of a field description with the lost of diffraction effects. A light ray is a path where the center of the electromagnetic energy flows and with a direction equal to the normal of the electromagnetic fields wave front. As a special case the analytical expression for the phase, amplitude and Doppler frequency can be found, if it can be assumed that the refractivity structure of the atmosphere is spherical symmetric. By applying the formula of Bouguer (Snell's law for a spherical stratified media) a simple analytical description can be obtained. The formula of Bouguer can be generalized to cover a non-spherical media, but in this case the inversion can not be done without pre-knowledge of the structure of the refractivity.

The validity of the optical geometrical description of radio occultation signals in the Earth atmosphere is due to the weak refractivity and that the gradients of the refractivity can be considered small in most cases. However in the case of a strong gradient of the refractivity it must be expected that the geometrical description brakes down. The theory needed for the geometrical optical description can be found in [Born&Wolf, 1999].

Depending on the structure of the refractivity several rays can be present at the same time. In this multipass situation the LEO receives a signal which is a sum of sub signals with different Doppler frequencies. This complicates the signal processing.

1.3 The phase and the Doppler frequency

The Phase of a single ray is given by

$$\psi = k\int_{s_G}^{s_L} n ds = k\left[\sqrt{r_L^2 - a^2} + \sqrt{r_G^2 - a^2} + a\alpha + \int_a^{\infty} \alpha(x)dx)\right] \tag{1}$$

where $a = Impact\ parameter,\ \alpha = Bending\ angle\ and\ r_L, r_G\ the\ LEO\ and\ the\ GPS\ radii$

It is seen that the phase has a memory term, the integral of the bending angle. This means that the phase of the occultation signal at all heights always include an ionosphere contribution.

The Doppler frequency for a single ray is given by

$$\omega(t) = \dot{\psi} = k(\frac{\dot{r}_G}{r_G}\sqrt{r_G^2 - a^2} + \frac{\dot{r}_L}{r_L}\sqrt{r_L^2 - a^2} + a\dot{\theta}) \tag{2}$$

where the dot's denotes time derivates.

2. Processing of occultation signals

Optimal signal processing means utilization of all available pre-knowledge of the physical nature of the signal.

- The signal is locally narrow banded i.e. by subtracting the vacuum phase the frequency bandwidth is down to 10Hz
- By using the synthetic aperture the frequency resolution can be optimized
- The instantaneous Doppler frequency is a decreasing/increasing function of time. In the case of multipass, several frequencies can be present at the same time.

If the signal is processed by an array of frequency filters and these gives a signal when a frequency is present, the recording of these temporal events will display the Doppler frequency as function of time. This means that a Fourier transforms of the signal will resolve multipass and give an optimal resolution.

The Fourier transform can be considered as a phasematching which select frequencies in the signal. The selection of the frequencies can be shown by using ***the stationary phase method***. If there are multiple stationary points i.e. the same frequency is present at several time points we have a situation which could be called temporal multipath. The temporal multipass can be caused by the non-radial path of the satellites and by horizontal gradients. Especially, the plain Fourier transform would give errors in the Doppler frequency curve when the satellite paths are non-radial.

In order to remove the temporal multipass a more general phasematching than the Fourier transform method can be sought.

2.1 Phasematching

The occultation signal $A(t)e^{i\psi(t)}$ is multiplied with the phasor, $e^{-i\psi_0(c,t)}$, where $\psi_0(c,t)$ is a phase depending on the parameter c. The result is integrated in time (or another variable which is a mapping of the time space):

$$\begin{aligned} u(c) &= \int_0^T A(t)e^{i(\psi(t)-\psi_o(c,t))}dt \\ &\cong \sqrt{\frac{2\pi i}{\ddot{\psi}(t_1)-\ddot{\psi}_o(c,t_1)}}A(t_1)e^{i[\psi(t_1)-\psi_o(c,t_1)]}\Big|_{\dot{\psi}(t_1)=\dot{\psi}_o(c,t_1)} \end{aligned} \tag{3}$$

The condition $\dot{\psi}(t_1)=\dot{\psi}_o(c,t_1)$ denotes a stationary point in time. If we, with the choice of $\psi_0(c,t)$ has accomplished that there only exists one stationary point at any time, the function $u(c)$ can explicit be represented by the approximation above.

The condition for absence of temporal multipath is

$$\ddot{\psi}(t)-\ddot{\psi}_0(c,t)\neq 0 \qquad \text{for} \quad 0<t<T \tag{4}$$

In the design of the phase $\psi_0(c,t)$ this conditions should be fulfilled. However this depends on the parameter to be measured and is therefore not possible in all cases. The search for the right matching phase, have resulted in the development of the ***Fourier***, the ***FSI*** and the ***Phasematching*** methods.

2.2 The generic methods of phasematching

The phase of $u(c)$, $\psi(t_1)-\psi_o(c,t_1)$, is a function of the parameter c, and by differentiating the phase with respect to c, an auxiliary function on parametrical form can be found:

$$\left[c,\frac{\partial(\psi-\psi_o)}{\partial c}\right]_{\dot{\psi}(t_1)=\psi_0(c,t_1)} \tag{5}$$

which expresses a functional relation between the parameter c and the partial derivative of the matching phase.

I: *The Fourier method* $\psi_0(c,t)=ct$

$$\left[c,\frac{\partial(\psi-\psi_o)}{\partial c}\right]_{\dot{\psi}(t_1)=\psi_0(c,t_1)}=[c,-t_1] \tag{6}$$

where c is related to the impact parameter through the Doppler equation:

$$c = k(a\dot{\theta} + \frac{\dot{r}_L}{r_L}\sqrt{r_L^2 - a^2} + \frac{\dot{r}_G}{r_G}\sqrt{r_G^2 - a^2}) \tag{7}$$

In the case where the radial velocities are zero, the impact parameter is directly proportional to Doppler frequency c.

II. *The FSI method:*

$$\left[c, \frac{\partial(\psi - \psi_o)}{\partial c}\right]_{\dot{\psi}(t_1)=\psi_0(c,t_1)} = [c, -t_1] \tag{8}$$

Method A, with the matching phase given by:

$$\psi_0(c, c_0, t) =$$
$$k(\sqrt{r_L^2 - c_0^2} + \sqrt{r_G^2 - c_0^2} - c_0(\tan(\frac{\sqrt{r_L^2 - c_0^2}}{c_0}) + \tan(\frac{\sqrt{r_G^2 - c_0^2}}{c_0})) + c\theta), \tag{9}$$

The impact parameter is found from the Doppler equation:

$$a\dot{\theta} + \frac{\dot{r}_L}{r_L}\sqrt{r_L^2 - a^2} + \frac{\dot{r}_G}{r_G}\sqrt{r_G^2 - a^2} = c\dot{\theta} + \frac{\dot{r}_L}{r_L}\sqrt{r_L^2 - c_0^2} + \frac{\dot{r}_G}{r_G}\sqrt{r_G^2 - c_0^2} \tag{10}$$

It is seen that the impact of the radial velocities are reduced with a proper choice of c_0

Method B, with the matching phase given by:

$$\psi_0(c,t) = k(ct + \int_0^t (\frac{\dot{r}_L}{r_L}\sqrt{r_L^2 - c_0^2(t)} + \frac{\dot{r}_G}{r_G}\sqrt{r_G^2 - c_0^2(t)})dt) \tag{11}$$

where $c_0(t)$ is a model of the impact parameter. A special case of this is $c_0(t) = a_0(t)n_0(a_0)$ where $a_0(t)$ is the vacuum impact parameter and n_0 the model of the refractivity.

Again, the impact parameter is found from the Doppler equation:

$$a\dot{\theta} + \frac{\dot{r}_L}{r_L}\sqrt{r_L^2 - a^2} + \frac{\dot{r}_G}{r_G}\sqrt{r_G^2 - a^2} = c\dot{\theta} + \frac{\dot{r}_L}{r_L}\sqrt{r_L^2 - c_0^2(t)} + \frac{\dot{r}_G}{r_G}\sqrt{r_G^2 - c_0^2(t)} \tag{12}$$

It is seen that the impact of the radial velocities are reduced overall with a proper choice of the model of c_0.

Other variations of the FSI method exists [Gorbunov&Lauritzen 2004]

III. *The Phasematching method*

$$\left[c, \frac{\partial(\psi - \psi_o)}{\partial c}\right]_{\dot{\psi}(t_1)=\psi_0(c,t_1)} = [c, \beta] \tag{13}$$

With the matching phase given by

$$\psi_o(c,t) = k\left(\sqrt{r_L^2 - c^2} + \sqrt{r_G^2 - c^2} + c\beta\right) \tag{14}$$

with $\beta = \theta - a\tan\left(\frac{\sqrt{r_L^2 - c^2}}{c}\right) - a\tan\left(\frac{\sqrt{r_G^2 - c^2}}{c}\right)$

Again, the impact parameter is found from the Doppler equation:

$$a\dot{\theta} + \frac{\dot{r}_L}{r}\sqrt{r_L^2 - a^2} + \frac{\dot{r}_G}{r_G}\sqrt{r_G^2 - a^2} = c\dot{\theta} + \frac{\dot{r}_L}{r}\sqrt{r_L^2 - c^2} + \frac{\dot{r}_G}{r_G}\sqrt{r_G^2 - c^2} \tag{15}$$

which gives $c = a$

The phasematching method solves the problem with the radial velocities perfectly. It gives directly the bending-angle as a function of the impact parameter. However the phasematching function is non-linear and the processing can't be implemented with a fast Fourier transform.

3. FSI implementation problems

The FSI method is fairly easy to implement. Test on simulated noise free occultation signals, gives good results. However, real signals are more difficult to process. They are noisy and contain sometimes detection errors. In the following the single steps in the processing chain will be described and discussed.

3.1 Implementation of the FSI processing

In this section technical issues in the implementation of the FSI method are addressed. The occultation signal is supposed to be given as amplitude and phase (the excess phase) sampled with 50 Hz. In the following the steps in the processing chain, used by the authors, will be explained and discussed.

1.The signal phase (the excess phase) is modified:
- The vacuum phase is added so the real signal phase is established
- The FSI phasematching phase is subtracted from the phase

2.The Amplitude is (optional) modified.
3.The center frequency of the now modified signal is found and a new signal is formed with a center frequency of zero.
4.The phase and amplitude of the new signal is upsampled 20-30 times depending on the bandwidth of the new signal.
5.The Fourier transform is performed with a FFT.
6.The differential of the phase with respect to frequency is computed giving the time of arrival spectrum.
7. From the selected time of arrival spectrum, the arrival time and successively the bending angle as function of the impact parameter is found.

These seven steps described do not involve any filtering. Step 6 involves a discrimination of the time of arrival spectrum, so only the information bearing part of the signal is left for further processing. This is described in the following section. After the discrimination a filtering of the signal has to be preformed. The filtering problem is complicated. A relatively simple method is to use an expansion in Chebyshev polynomials [E.T. Goodwin, 1961], which both gives an interpolation and a smoothing of the functions. This is convenient, but the essential documentation of the final spatial resolution is missing. A deeper analysis and a solution of the problem will be given in Sec. 3.3.

3.2 Discrimination of the time of arrival spectrum

The differential of the phase spectrum (the time of arrival spectrum), which is proportional to

spectrum of the "arrival" times of the rays, consists of a signal area with noise plus a pure noise area (see Fig. 1). The task now is to separate the signal from the pure noise. Several methods for this have been investigated: Discrimination of the FSI spectrum amplitude, discrimination of the time of arrival spectrum and a new method which use amplitude discrimination together with a discrimination base on comparison of two different orders of differential operators.

The experience with the amplitude discrimination was that it was difficult to get a robust and reliable method, which preserved an optimum amount of information of the signal. The discrimination of the time of arrival spectrum is done by computing a mean local spread (the spread is calculated with in a window) as function of the frequency.
The local phase difference spread is high in areas with noise and low in areas where the signal is present. With a proper threshold, the areas with noise can be separated from the signal. If the threshold is too large to much noise from the two ends of the signal will be taken into account in the further signal processing and if it is to low the signal will be truncated. The establishment of the threshold is therefore always a compromise. Another complication is that the "optimum" threshold varies for each occultation. The solution to this problem has here been to compute the mean sum of the above mentioned local spreads and choose the threshold as a fraction of this sum. This appears to be a fairly reliable and robust method for establishing the threshold for a large number of real occultation data. With the threshold the start and end of the occultation can be found i.e. the information bearing part of the signal can be isolated. The signal does still contain receiver noise and numerical noise from the finite discrete Fourier transform. This noise can partly be filtered out on the cost of a reduced spatial resolution.

The third method of noise discrimination is a combination of amplitude threshold and the use of two different operators for a numerical differentiation of a signal. The outcome of the two ways to do the numerical differentiation should be very close if the signal is 'well' behaved. However if the signal consist of pure noise the two (different) numerical differentiators cannot be expected to give the same result. The differential operators use here are given in Eq. x1 and x2. The first is the well known formula for a two points numerical differentiation.

$$y_0' = \hat{D}_2 y = (y_1 - y_0)/h, \tag{x1}$$

where $h = x_1 - x_0$. The numerical truncation error is given by $hy''(\xi)/2$ where ξ is lying in the interval $[x_1, x_0]$. The second differential operator is a seven point algorithm given by:

$$y_0' = \hat{D}_7 y = (y_3 - 9y_2 + 45y_1 - 45y_{-1} + 9y_{-2} - y_{-3})/60h \tag{x2}$$

The numerical truncation error is here $h^6 y^{(7)}(\xi)/140$.
According to the remarks above we must expect that the measure $\left|(\hat{D}_7 - \hat{D}_2)y\right|$ is ≈ 0, when a well behaved signal y, is present and $>>0$ when a pure noise signal y, is present. If the signal y consist of an information bearing signal S, plus a noise part N (independent of the signal) the difference measurer $\left|(\hat{D}_7 - \hat{D}_2)(S+N)\right| \cong \left|(\hat{D}_7 - \hat{D}_2)N\right|$ will always be $>>0$, and the method can consequently not be used for noise discrimination purpose. However, in case of non-additive noise, for instance if we have a complex signal consisting of a information bearing part and additive noise, the discrimination method will work on the amplitude and phase where the noise is a non-additive part. In this specific case the phase spectrum from the FSI method has the form (to first order in the signal-to-noise ratio):

$$\varphi = \begin{cases} \varphi_0 - \dfrac{N}{S}\sin(\varphi - \psi) & \textit{when a signal is present} \\ \psi & \textit{when only noise is present} \end{cases} \tag{x3}$$

where φ is the phase of the FSI spectrum, φ_0 the information bearing phase and ψ the phase from the noise. S and N is amplitudes from the information bearing part of the signal and the noise respectively.

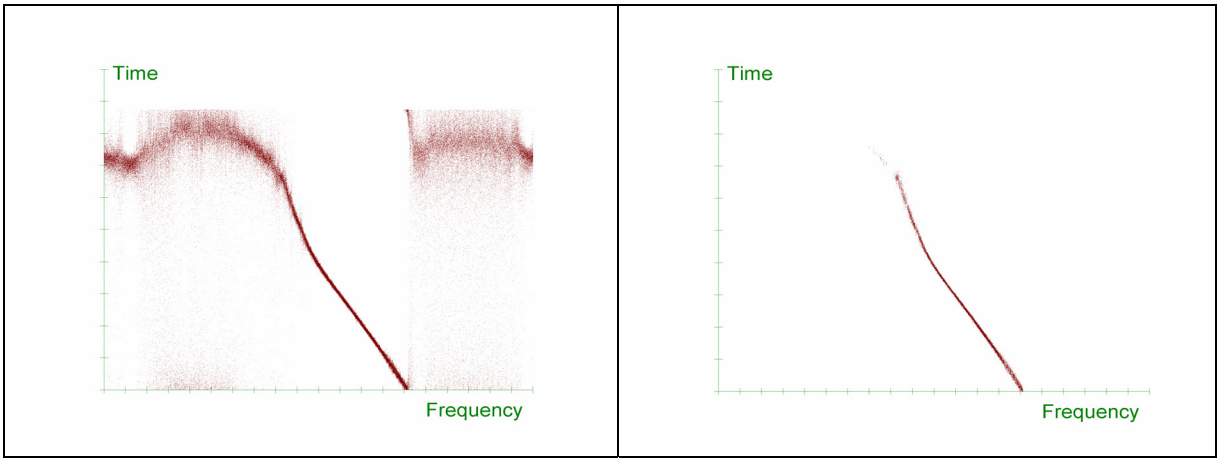

Figure 1
The time of arrival spectrum from real CHAMP data. The left image shows the raw spectrum and the right shows the discriminated spectrum.

Applying $(\hat{D}_7 - \hat{D}_2)$ on the phase (Eq.x3) the result yields:

$$\left|(\hat{D}_7 - \hat{D}_2)\varphi\right| = \begin{cases} \left|(\hat{D}_7 - \hat{D}_2)(\varphi_0 - \frac{N}{S}\sin(\varphi - \psi))\right| \approx 0 \\ \left|(\hat{D}_7 - \hat{D}_2)\psi\right| >> 0 \end{cases} \quad \text{(x4)}$$

From Eq.x4 it is seen that the area with pure noise is identified. In single cases, $\left|(\hat{D}_7 - \hat{D}_2)\psi\right| \approx 0$ so additional discrimination has to be performed, here by using amplitude threshold.

In Fig. 1 the results of the discrimination is shown. The amplitude threshold was set to the half of the mean amplitude of the FSI spectrum. The phase noise threshold was set to 1/100. The actual threshold values were not critical, and have shown to work on a random collection of CHAMP data. As seen from Fig.1 the information bearing part of the signal is clearly identified. Other effects are that some points in the information part, where the noise is dominating, also are filtered out. This can be difficult to see on the actual curve, but is clearly observed at lager magnification.

The signal discriminating method used here has several advantages; it isolated the wanted information without changing or destroying the resolution and computational it is fast. Other applications of this method could be thought, for instance within image recognition, but this is outside the scope of this report.

3.3 Filtering and spatial resolution

In the time of arrival spectrum (the phase difference spectrum Fig.1) fluctuations in the arrival times causes large fluctuations in the bending angle i.e. for real data fluctuations up to 1 mrad has been seen unless smoothing and averaging was done on the data. Averaging of data is a legal way to process data as long as the variance of the data is reported. In this case the problem is that we want

to know the uncertainty in the frequency or spatial domain and not in the time or bending angle domain. For real data sampled with 50 Hz, the time of arrival of the rays will have a basic uncertainty of 20 msec, and the upsampling of the signal to 1000 Hz or larger will only give a pseudo time of arrival resolution of 1 msec or better. The thermal noise in the original signal is also upsampled which means that the noise is correlated in the pseudo sample intervals. The discrete nature of the FFT and the transform of the noise into a multiplicative phase noise in the spectrum, give both contributions to the time of arrival noise. The deterministic variation of the time of arrival is given by the persistence time [Jensen et al., 2003b] i.e. the time interval in which the Doppler frequency is approximately constant. Usually the persistence time is larger than the 20 msec sampling interval (this is the basic for choosing 50 Hz sampling in radio occultation) and one must expect that only a finite number of discrete frequencies are present in a sample. If there is a distribution of frequencies this must be due to thermal noise, sample noise and processing noise as mentioned above.

Now, from this analysis a filtering scheme can be proposed. If the time of an arrival function $t(\omega)$ is considered to be in N intervals $t_i < t < t_i + \Delta t$ where $t_0 = 0$ and $t_{N-1} = T$ (the recording time of the occultation) then we can define a function $\xi_i(\omega)$ with the following properties:

$$\xi_i(\omega) = \begin{cases} 1 & if \quad t_i < t(\omega) < t_i + \Delta t \\ 0 & else \end{cases} \tag{16}$$

Δt can naturally be chosen as the sampling time for the actual occultation.

In order to illustrate the possible behavior of $\xi_i(\omega)$ in a time interval i the following graphic are shown: The vertical bars indicate that $\xi_i(\omega) = 1$

1. || → *frequency*
2. ||| || → *frequency*
3. ||||||| → *frequency*
4. ||| || || → *frequency*

In example 1, two frequencies occur in the time interval i. The frequencies are close together and the spread is small. In 2, clusters of frequencies are seen, which can be interpreted in two ways. Either the spread in frequencies are large or we have a multipass situation. In 3, clusters of frequencies are seen. The spread is probably large. In 4, three distinct clusters of frequencies are seen which indicate a clear multipass situation. Using the function $\xi_i(\omega)$ the local mean and spread with respect to ω can be computed and the arrival time function $t(\omega)$ can then be transformed to a discrete function or a table $[t_i, <\omega>; \sigma_\omega]$ with the time and the mean local Doppler frequency as the variables and with the local mean spread as a parameter. This table can then be used to calculate the bending angle as function of the impact parameter and by mapping the local mean spread of the Doppler frequency into and uncertainty in the impact parameter (σ_a) i.e.

$$[t_i, <\omega>; \sigma_\omega] \rightarrow [\alpha_i, <a>; \sigma_a] \tag{17}$$

The local means and spread can only be calculated in the case of possible multipass if certain constrains are imposed. This is seen from example 2 and 3 above.

The width of a multipass can in principle be zero, however in this limit it will not be possible to distinguish between a real multipass and a one induced by noise. Consequently, we have to make a constrain saying that we only accept a separation between clusters which is larger than a certain $\Delta\omega$ (Δa) before it can be accepted as a (possible) multipass. The choice Δa will be discussed at

the end of Sec. 3.3.1.

In order to compute the local mean(s) and spread(s) $\xi_i(\omega)$ is correlated with a square shaped function $s(\omega)$ of the width $\Delta\omega$ (Eq.18).

$$\Gamma_i(\omega) = \int_{\omega_{\min}}^{\omega_{\max}} s(\omega - \omega', \Delta\omega)\xi_i(\omega')d\omega' \tag{18}$$

The peaks of the correlation function $\Gamma_i(\omega)$ give the local means and the local spread can be defined in various ways: as the half width of the peak, the radius of curvature of the peak or the spread of the peak. The correlation technique is however impractical from an implementation point of view and should only serves as a picture of the filtering problem. In the next section (Sec. 3.3.1) a practical implementation will be described.

In [Gorbunov et al., 2005] the uncertainty of the Doppler frequency is evaluated by using running Fourier transforms. This method is questionable though it will produce a estimate of the Doppler uncertainty. The question is how this measure is related to the 'real' Doppler spread in the FSI function $t(\omega)$. First, the time length of this local Fourier transform gives an intrinsic uncertainty in the spread around the peak maxima in the Fourier amplitude spectrum. Secondly, the impact of the noise will be different from the noise impact in the FSI spectrum. Third, the numerical noise due to the short length of the discrete Fourier transform will also give a contribution to the spread or uncertainty in the Doppler frequency. In the best case the running Fourier method will give a very conservative measure of the uncertainty.

3.3.1 Implementation of the Filtering

Instead of the correlation technique suggested above, the following method will be applied. In the time interval $t_i < t < t_i + \Delta t$ the impact parameter(s) are computed i.e. the frequency space is mapped into the impact parameter space at the given time interval. The results are store into an array marked with the time t_i i.e. $[t_i; a_1, a_2 .....a_p]$, p denotes the number of rays arriving in the time interval $t_i < t < t_i + \Delta t$. The array is now sorted in ascending order i.e. $[t_i; a_1, a_2 .....a_p] \rightarrow [t_i; a_{\min(1)}, ...a_{\max(p)}]$. By taking the difference between two neighbors in the array $[t_i; a_2 - a_1, a_3 - a_2, ...a_p - a_{p-1}]$ and applying the rule that if the difference is larger than Δa (the user defined spatial resolution) a new ray is present. An example of this: If $a_2 - a_1 < \Delta a$ and $a_3 - a_2 > \Delta a$ then a_1, a_2 can be considered to be one ray and a_3 is the start of a second ray. The mean $(< a >)$ and spread (σ) for each ray is computed. The result is stored in a new array $[t_i; < a_1 >, \sigma_1, < a_2 >, \sigma_2 .....]$ where the number of pairs $(< a >, \sigma)$ is the number of possible multipass. With the knowledge of the satellite path at the time t_i the bending angle can be computed from the angular equation for each pair $(< a >, \sigma)$. The result form these processing steps is a table $[a, \alpha]$ giving the impact parameter as function of the bending angle. As mentioned above we have only identified possible multipass. By mapping $[a, \alpha]$ we will see transients in the curve which is smaller than Δa and it is therefore allowable to make an averaging over the length Δa. This completes the filtering process.

The description of the filtering process given above could as a whole seems complicated. However, the algorithms are fast, so with the present computer speed the whole process, the FSI, the noise discrimination and the filtering can be done within 1 sec for both L1 and L2 and with the ionosphere corrected impact parameter as function of the bending angle as the final result.

The problem with the filtering is the choice of Δa . An optimum value of Δa cannot be exactly determined. From simulated noise free occultation signals a minimum value of Δa can be estimated, which takes care of the numerical errors in the FSI method. This is discussed in Sec.4.

Another way to estimate the magnitude of Δa is to look at the physical atmosphere. In the lower part of the atmosphere the spatial changes can be fast whereas in the upper part of the atmosphere $(>10Km)$ the changes must be expected to be slow and resolution in the range of kilometers satisfactory. This calls for an averaging which depends on the height.

It should be noted that user defined quantity Δa has double meaning in this: it is first the allowable width of the occurred multipasses and secondly the averaging length. In the case of a variable averaging, $\Delta a = \Delta a_0$ is constant during the filtering but varying during the averaging from Δa_0 at low heights to a higher value at larger heights.

3.4 The phase noise in the FSI spectrum

In appendix I the impact of thermal noise on the arrival time are calculated. The main result here is the variance of the time of arrival (Eq. I17). It yields

$$\langle(\partial t^2\rangle \cong T^2 \frac{1}{\pi\Gamma}((\frac{t_1}{T})^2 + \frac{1}{4\pi}\frac{1}{\Delta fT}) \qquad (19)$$

where $\Gamma = A_0^2 / E_0 \Delta f$ is the square of the signal-to-noise ratio in the Fourier space (∂t and t_1 are introduced in the introduction of the appendix). The product $E_0 \Delta f$ is the noise energy in the frequency band and ΔfT is the time-bandwidth product. In the FSI method this last quantity will usual be a large quantity. The uncertainty increases at the end of the occultation due to the decrease of the actual signal-to-noise ratio. The equation is an approximation which is valid in the limit of large signal-to-noise ratios. It is seen that the relative variance is constant for large time of arrivals.

4. FSI processing of real data and simulations

In order to test the FSI processing method simulations are useful. The test signals generated here are done with the use of a geometrical optical propagator and with satellites in circular orbits. Diffraction effects are consequently not present in the signal and detection errors and noise due to the phase locked loop are also absent. However, numerical noise due to the discrete nature of FFT applied in the FSI method will be visible and by adding thermal noise the robustness of the FSI to this type of noise will be revealed. The processing speed of the chain, from the reading of the (CHAMP) data to the computing of the ionosphere corrected bending angle, takes 1-1.5 sec. with the present 2.8 GHz computer.

In Fig. 2 an occultation with a distinctive multipass is generated. The top graph in Fig.2 shows the generated signal, the middle graph the discriminated time of arrival spectrum and the bottom graph show the measure impact parameter as function of the bending angle. The measured bending angle as function of the impact parameter is visually compared with the same function computed from the basic refractivity profile. The measured curve followed the compute curve in general but distinctive spikes are present in the measured curve. An averaging of $\Delta a = 50m$ seem to give a smooth bending angle which are visually identical to a reference curve which has been used for the generation the signal. By adding thermal noise to the occultation signal (see Fig.3, 4), the $50m$ is still sufficient at low heights, but at larger heights an averaging length of $300m$ makes the measured curve visually identical to the reference curve. In this last case the noise level is very high as seen in Fig.4. In the simulation no filtering in the sense described in Sec.3 has been performed due to the sampling

rate of $1000Hz$ for the simulated signal, so the considerations here are only related to the averaging of numerical and thermal noise.

In Fig. 5, 6 and 7 three examples of processing of real occultation data are shown. In the first example (Fig. 5) two filtering lengths have been applied $\Delta a = 100m$ and $\Delta a = 200m$. It is seen that the fine structure in the bending angle is more pronounced with the small filtering length. The fine structure could be real or caused by various sources of noise, so the choice of Δa is not a clear objective choice. In the simulations $\Delta a = 50m$, was sufficient even with moderate thermal noise. In order to get a better estimate of the filtering length simulation with all possible noise sources should be done.

The overall accuracy or the spread of the measurement (Fig.5, 6 and 7 left) reflects the magnitude of the filtering length, whereas the detail structures reflect the local spread.

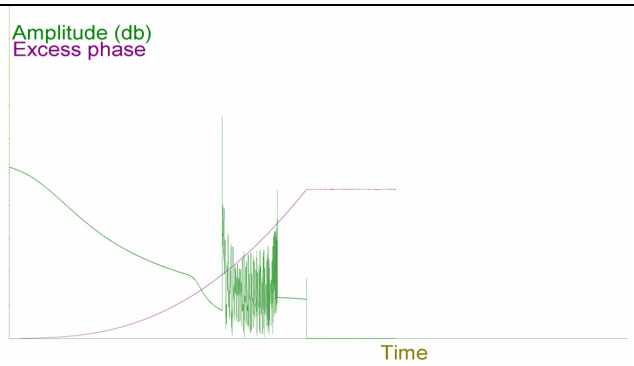

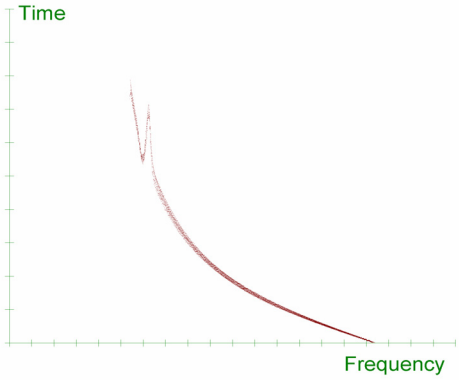

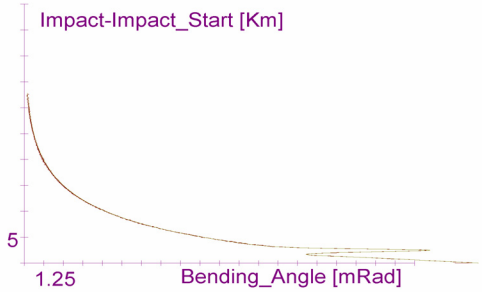

Figure 2

The FSI processing chain on a simulated signal with **low** noise content.

Top: Simulated radio occultation signal with a sampling rate of 1000Hz with a low amount of additive thermal noise. **Middle:** The time of arrival of the rays from the radio occultation signal at the left. The curve displayed the differentiation of the FSI phase with respect to frequency. The signal is discriminated, so only the information bearing part is present. **Bottom:** The impact parameter as function of the bending angle compared with a reference curve. The result is averaged equivalent to a resolution of 50 m. With this averaging the reference curve and the measured curve are nearly identical as seen.

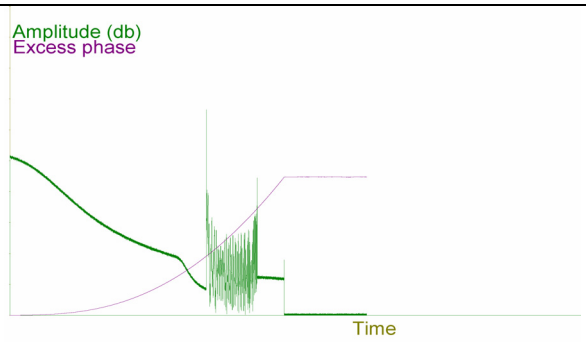

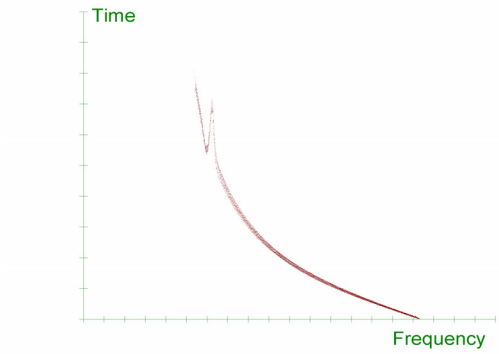

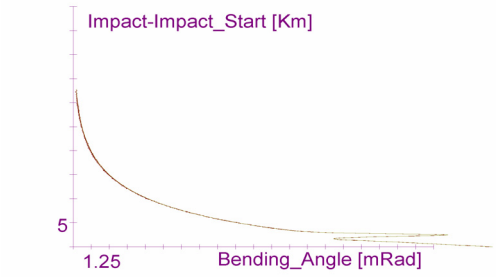

Figure 3
The FSI processing chain on a simulated signal with **medium** noise content.
Top: Simulated radio occultation signal with a sampling rate of 1000Hz with a medium amount of additive thermal noise. **Middle:** The time of arrival of the rays from the radio occultation signal at the left. The curve displayed the differentiation of the FSI phase with respect to frequency. The signal is discriminated, so only the information bearing part is present. **Bottom:** The impact parameter as function of the bending angle compared with a reference curve. The result is averaged equivalent to a resolution of 50 m. With this averaging the reference curve and the measured curve are nearly identical as seen.

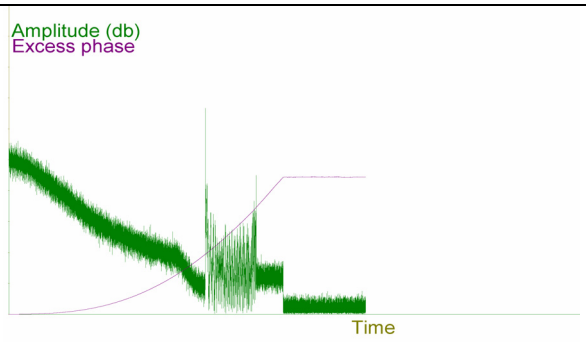

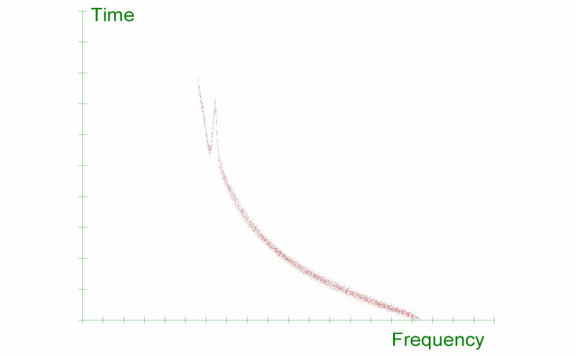

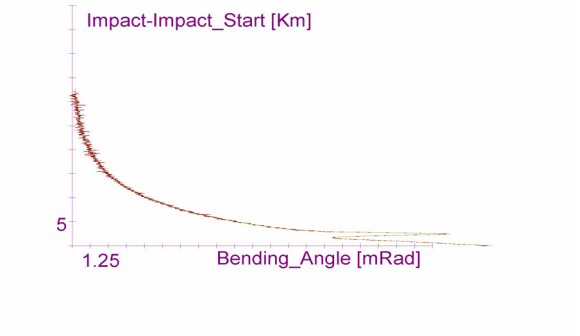

Figure 4

The FSI processing chain on a simulated signal with **high** noise content.

Top: Simulated radio occultation signal with a sampling rate of 1000Hz with a high amount of additive thermal noise. **Middle:** The time of arrival of the rays from the radio occultation signal at the left. The curve displayed the differentiation of the FSI phase with respect to frequency. The signal is discriminated, so only the information bearing part is present. **Bottom:** The impact parameter as function of the bending angle compared with a reference curve. The result is averaged equivalent to a resolution of 50 m. It is seen that impact of the noise is largest at high altitudes whereas the reference curve and the measured curve are identical at low altitudes. With an average length of 300 m the curves are practical identical (not shown).

In Fig. 6 and 7 a filtering length of 200m has been used. The averaging has been done with an exponential varying length form 200m at low altitude and up to 2000m at high altitudes. Despite the relatively large filtering length details are still present in the bending angle, which if the choice of the filtering length is correct must be interpreted as real feature in the measured bending angle. The bending angle from L2 in Fig. 7 looks disturbed probably due to the known low quality of the L2 signal.

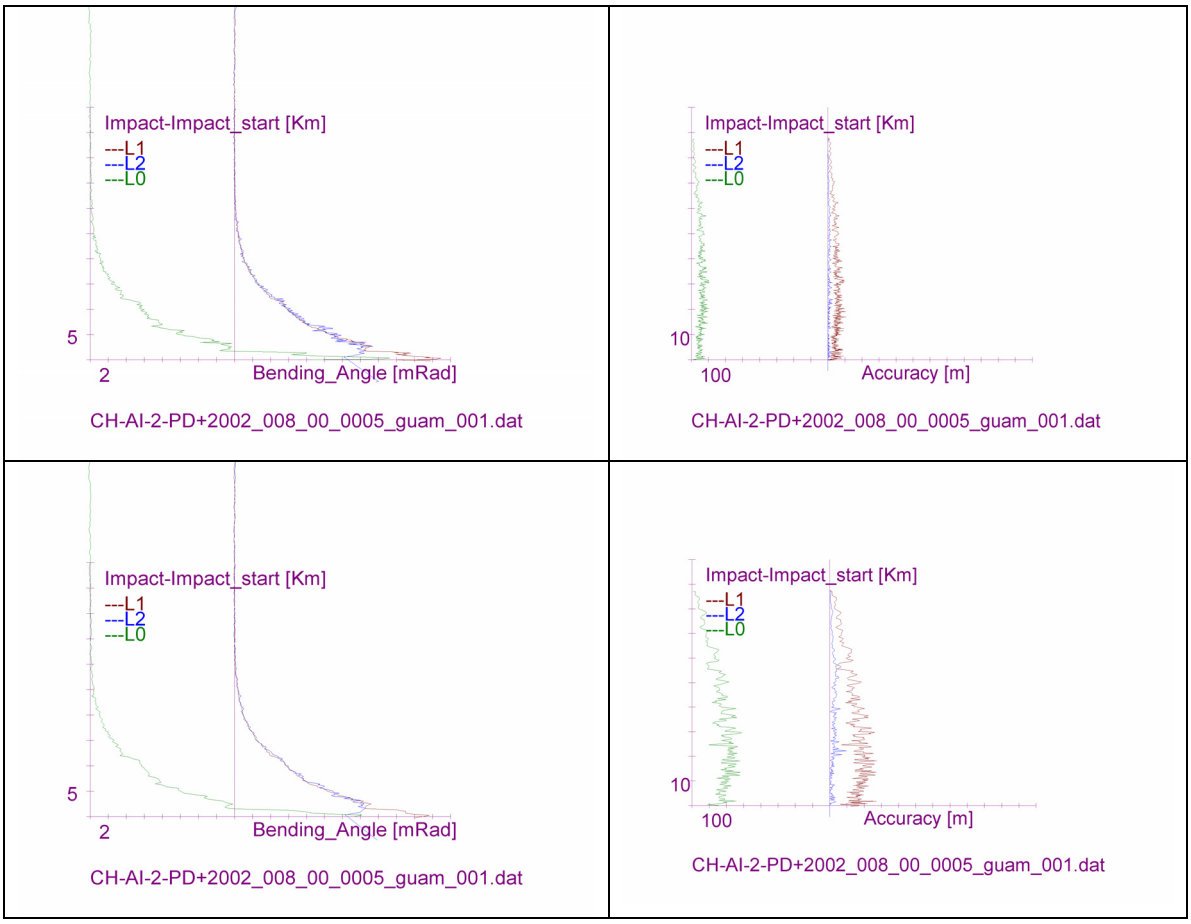

Figure 5

FSI processing of CHAMP data, first example. **Top left**: The measured impact parameter as function of bending angle. The red and blue curve is the result of the processing of L1 and L2 respectively. The green curve is the ionosphere corrected bending angle. L1 and L2 are separated for L0 with an offset. The filtering length is 100 m and the averaging length goes from 100 m at the minimum impact parameter to 1000 m at the maximum impact parameter. **Top right:** The measured accuracy from the filtering, L1 and L2 are separated form L0 with an offset. **Bottom right and left:** The same layout as for the top images. The filtering length is here 200 m and the averaging is going from 200 m to 2000 m.

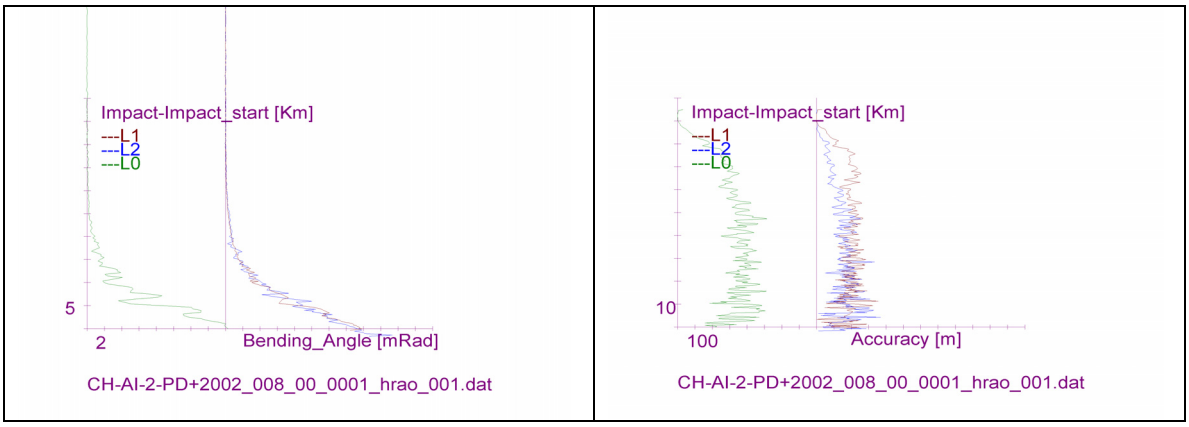

Figure 6

FSI processing of CHAMP data, second example. **Left**: The measured impact parameter as function of bending angle. The red and blue curve is the result of the processing of L1 and L2 respectively. The green curve is the ionosphere corrected bending angle. L1 and L2 are separated for L0 with an offset. The filtering length is 200 m and the averaging length goes from 200 m at the minimum impact parameter to 2000 m at the maximum impact parameter. **Right:** The measured accuracy from the filtering, L1 and L2 are separated form L0 with an offset.

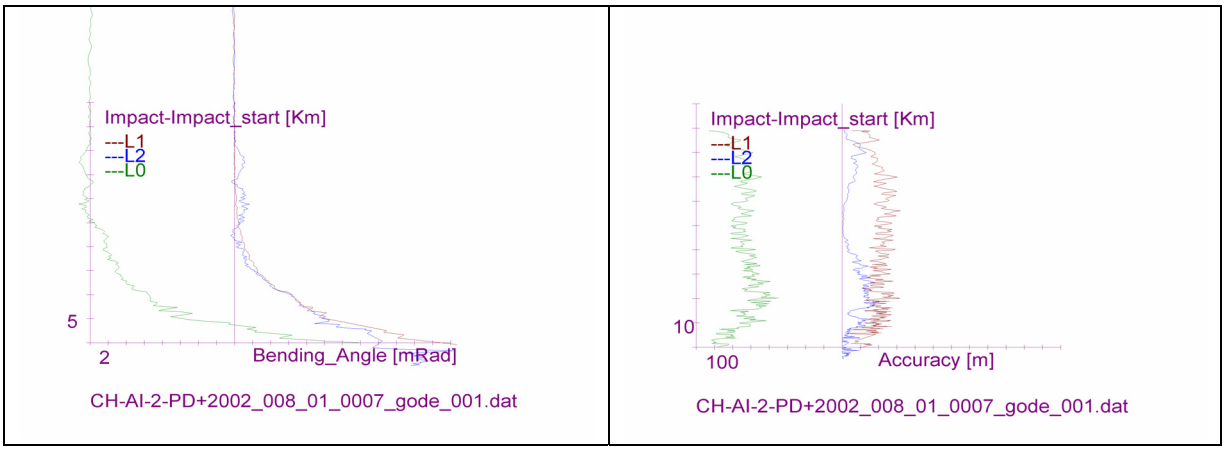

Figure 7

FSI processing of CHAMP data, third example. **Right**: The measured impact parameter as function of bending angle. The red and blue curve is the result of the processing of L1 and L2 respectively. The green curve is the ionosphere corrected bending angle. L1 and L2 are separated for L0 with an offset. The filtering length is 200 m and the averaging length goes from 200 m at the minimum impact parameter to 2000 m at the maximum impact parameter. **Left:** The measured accuracy from the filtering, L1 and L2 are separated form L0 with an offset. In this case it is seen that result from the L2 processing show some anomalies due to the known low quality of the L2 signal. The bending angle for L0 becomes negative at range of 30-40 km, which clearly is unphysical.

5. Conclusion

An overview of the present development of the FSI method has been given. The method proposed in Sec.3.2 converts the time of arrival uncertainties into uncertainties in the Doppler frequency. The method has the advantage that it operates directly on the measured arrival time as function of the Doppler frequency taking the available pre-information into account. The analysis shows that an improvement in the spatial resolution of the refractivity profile can be archive if the sampling rate is increased.

The result from the phase noise analysis (Sec. 3.3) can theoretically be use to extend the method if the arrival time spread (see Eq.19) is used to define varying time intervals. However this will demand longer computation times and will only be exact in case of simulations.

Acknowledgement
This work has partly been supported by EUMETSAT GRAS SAF through a visiting science program in cooperation with UK Met-office.

Appendix I: The impact of thermal noise in the FSI processing method.

In this appendix, the effect of thermal additive noise on the retrieval of the refractive index from occultation measurements will be analysed. It is assumed that the processing of the signal is done with the FSI method [*Jensen et al*, 2003]. The outlines for this analyse is:

- A description of the Fourier transform of band-pass filtered noise
- A calculation of the mean value and variance of the frequency derivate of the phase of the Fourier transform.

The FSI method gives as output the Doppler frequency as function of time. From the Doppler frequency, the impact parameter a, and the bending angle α can be derived. The Doppler frequency is the frequency of the Fourier transform and the time is found by differentiating the phase $\phi(\omega)$ of the Fourier transform i.e. $t_1 = -d\varphi(\omega)/d\omega$ (see [*Jensen et al.*, 2003a]). The uncertainty in the time determination ∂t, gives an uncertainty in the impact parameter ∂a. The relation is simply given by $\partial a = (da/dt)\delta t$. The mean value of δt and its variance are calculated in appendix I.2 for additive band-pass filtered noise.

The effect of the Fourier transformed noise, are the issues in appendix I.1. This section can be skipped, if the reader accepts the application of the results in appendix I.2.

I.1 Bandpass filtered noise

In order to describe the impact of the noise we will first define and describe the properties of the band pass filtered noise, which is the result of the pre-processing of the signal. The noise is passing in the band pass $\pm \frac{1}{2}\Delta\omega$ around the center frequencies q and $-q$. The noise contribution around q is denoted by N^+ and around $-q$, N^-.

$$N^+(t) = \frac{1}{2\pi}\int_{q-\frac{1}{2}\Delta\omega}^{q+\frac{1}{2}\Delta\omega} n(\omega)e^{i\omega t}dt = e^{iqt}\int_{-\frac{1}{2}\Delta\omega}^{\frac{1}{2}\Delta\omega} n(\omega+q)e^{i\omega t}d\omega$$
$$N^-(t) = \frac{1}{2\pi}\int_{-q-\frac{1}{2}\Delta\omega}^{-q+\frac{1}{2}\Delta\omega} n(\omega)e^{i\omega t}dt = e^{-iqt}\int_{-\frac{1}{2}\Delta\omega}^{\frac{1}{2}\Delta\omega} n(\omega-q)e^{i\omega t}d\omega \qquad \text{(I1)}$$

The total noise $N(t) = N^+ + N^-$ can be expressed as a sum of cosine and sine functions, as shown below:

$$N(t) = N^+ + N^- = N_C(t)\cos(qt) - N_S(t)\sin(qt)$$

where

$$N_C(t) = \frac{1}{2\pi}\int_{-\frac{1}{2}\Delta\omega}^{\frac{1}{2}\Delta\omega}(n(\omega+q)+n(\omega-q))e^{i\omega t}d\omega \qquad \text{(I2)}$$
$$N_S(t) = -\frac{i}{2\pi}\int_{-\frac{1}{2}\Delta\omega}^{\frac{1}{2}\Delta\omega}(n(\omega+q)-n(\omega-q))e^{i\omega t}d\omega$$

The pair (N_C, N_S) can be considered as a pair of noise signals in quadrature.
The noise function $K = N_C + iN_S$ is a function of time. In the following, the noise considerations are done in the Fourier space and for that reason; the properties of the finite Fourier transform of K

will be analyzed. The mean value of K and $dK/d\omega$ and there variances will be calculated, with the intension of using the result to determined the mean and variance of the impact parameter.

$$\begin{aligned} K(\omega) &= \frac{1}{T}\int_{-T/2}^{T/2} K(t)e^{-i\omega t}dt \\ &= \frac{1}{\pi}\int_{-T/2}^{T/2} e^{-i\omega t}\int_{-\frac{1}{2}\Delta\omega}^{\frac{1}{2}\Delta\omega} n(\omega'+q)e^{i\omega' t}d\omega' dt \\ &= \frac{T}{\pi}\int_{-\frac{1}{2}\Delta\omega}^{\frac{1}{2}\Delta\omega} n(\omega'+q)\frac{\sin\frac{1}{2}(\omega'-\omega)T}{\frac{1}{2}(\omega'-\omega)T}d\omega' \end{aligned} \tag{I3}$$

where T, the time length of the signal.

It is seen that

$$\langle K(\omega)\rangle = 0 \tag{I4}$$

The variance of the spectral noise becomes:

$$\langle |K(\omega)|^2\rangle \cong \frac{1}{\pi^2}E_0\Delta\omega = \frac{2}{\pi}E_0\Delta f \tag{I5}$$

where E_0 is the noise energy per frequency.
The derivate of the Fourier noise with respect to ω yields:

$$\frac{dK(\omega)}{d\omega} = \frac{1}{\pi}\int_{-\frac{1}{2}\Delta\omega}^{\frac{1}{2}\Delta\omega} n(\omega'+q)\frac{d}{d\omega}\left(\frac{\sin\frac{1}{2}(\omega'-\omega)T}{\frac{1}{2}(\omega'-\omega)T}\right)d\omega' \tag{I6}$$

It is easily seen that the mean value of the noise derivative is zero. The variance of this yields:

$$\begin{aligned} \left\langle\left|\frac{dK(\omega)}{d\omega}\right|^2\right\rangle &= \frac{E_0}{\pi^2}\int_{-\frac{1}{2}\Delta\omega}^{\frac{1}{2}\Delta\omega}\left(\frac{d}{d\omega}\left(\frac{\sin\frac{1}{2}(\omega'-\omega)T}{\frac{1}{2}(\omega'-\omega)T}\right)\right)^2 d\omega' \\ &= \frac{E_0T^2}{4\pi^2}\int_{-\frac{1}{2}\Delta\omega}^{\frac{1}{2}\Delta\omega}\left(\frac{\sin\frac{1}{2}(\omega'-\omega)T - \frac{1}{2}(\omega'-\omega)T\cos\frac{1}{2}(\omega'-\omega)T)}{(\frac{1}{2}(\omega'-\omega)T)^2}\right)^2 d\omega' \\ &= \frac{E_0T}{2\pi^2}\int_{\frac{1}{2}(T\omega-\frac{1}{2}T\Delta\omega)}^{\frac{1}{2}(T\omega+\frac{1}{2}T\Delta\omega)}\left[\frac{\sin(x)-x\cos(x)}{x^2}\right]^2 dx \end{aligned} \tag{I7}$$

The resulting integral above cannot be expressed explicit as function of ω and $\Delta\omega$, but the result can been described approximated. To do this the function $U(x)$, defined below, has been calculated analytical and the result is displayed on the graph below.

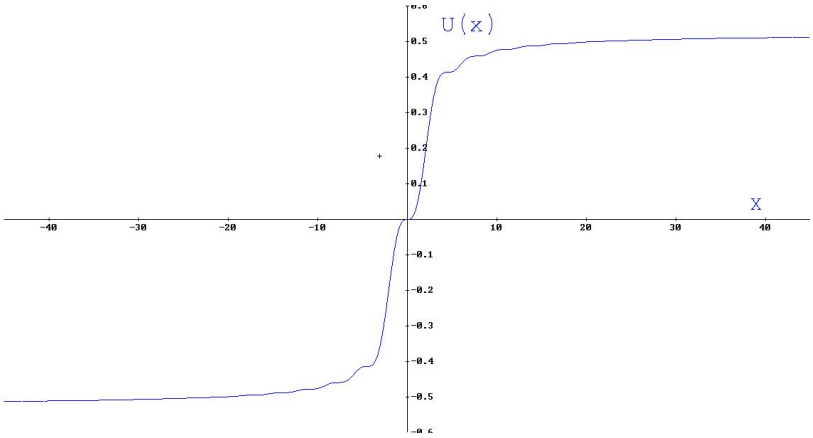

$$U(x) = \int_0^x \left[\frac{\sin(t) - t\cos(t)}{t^2} \right]^2 dt \tag{I8}$$

It is seen that the function is a two-valued function with a narrow transition area around zero. The transition area is as seen from the graph approximately restricted by $|x| \le 10$. In the calculation of the noise term, due to the derivate of the noise, the difference between $U(\frac{1}{2}\omega T + \frac{1}{4}\Delta\omega T) - U(\frac{1}{2}\omega T - \frac{1}{4}\Delta\omega T)$ has to be approximated. First it is seen that if $|\omega| \ge \frac{1}{2}\Delta\omega$ the contribution will be approximately zero. This is also to be expected from a physical point of view, due to bandpass nature of the noise. If $|\omega| \le \frac{1}{2}\Delta\omega$, the contribution will approximately be 1, by near the narrow areas where the transition occurs. However since these points always will give a contribution smaller than 1, we do make a conservative estimate by setting these contributions equal to 1.

$$\left\langle \left| \frac{dK(\omega)}{d\omega} \right|^2 \right\rangle \cong \begin{cases} \frac{E_0 T}{2\pi^2} & |\omega| < \frac{1}{2}\Delta\omega \\ 0 & |\omega| > \frac{1}{2}\Delta\omega \end{cases} \tag{I9}$$

I.2 Mean value and variance of the Fourier phase frequency derivate.

The output of the FSI method, the Fourier transform of the signal plus noise, can be written as:

$$F(\omega) = |F(\omega)| e^{i\varphi(\omega)} = A_0 e^{i\varphi_0(\omega)} + K(\omega) \tag{I10}$$

where A_0 is the amplitude of the Fourier transform. A_0 is a constant or a weak function of the frequency in case of absorption in the atmosphere, so it is safe to considered it to be a constant. $\phi(\omega)$ is the phase of the Fourier transform and $\phi_0(\omega)$ is the Fourier phase of the noise free radio occultation signal.

The Fourier phase is given by:

$$\varphi(\omega) = A\tan\left(\frac{A_0 \sin(\varphi_0) + \mathrm{Im}(K)}{A_0 \cos(\varphi_0) + \mathrm{Re}(K)}\right) \tag{I11}$$

The derivative of the detected Fourier phase yields:

$$\frac{d\varphi}{d\omega} = \frac{(A_0^2 + A_0\,\mathrm{Im}(K)\sin(\varphi_0) + A_0\,\mathrm{Re}(K)\cos(\varphi_0))\frac{d\varphi_0}{d\omega}}{|F(\omega)|^2}$$
$$+\frac{A_0(\cos(\varphi_0)\frac{d\,\mathrm{Im}(K)}{d\omega} - \sin(\varphi_0)\frac{d\,\mathrm{Re}(K)}{d\omega}) +}{|F(\omega)|^2} \qquad \text{(I12)}$$
$$\frac{\mathrm{Re}(N)\frac{d\,\mathrm{Im}(K)}{d\omega} - \mathrm{Re}(N)\frac{d\,\mathrm{Im}(K)}{d\omega}}{|F(\omega)|^2}$$

Expanding the equation above to $(A_0)^{-1}$ yields:

$$\frac{d\varphi}{d\omega} \cong (1 - \frac{1}{A_0}(\mathrm{Im}(K)\sin(\varphi_0) + \mathrm{Re}(K)\cos(\varphi_0)))\frac{d\varphi_0}{d\omega}$$
$$+\frac{1}{A_0}(\cos(\varphi_0)\frac{d\,\mathrm{Im}(K)}{d\omega} - \sin(\varphi_0)\frac{d\,\mathrm{Re}(K)}{d\omega}) + ... \qquad \text{(I13)}$$

From this the mean value of the detected time can be calculated.

$$\langle\frac{d\varphi}{d\omega}\rangle \cong \frac{d\varphi_0}{d\omega} \qquad \text{(I14)}$$

It is seen that the time $t_1 = -d\varphi(\omega)/d\omega$, is bias free. This is important, in that respect that a bias not will be present in the retrieval of the refractivity.

The calculation of the variance of the detected time is done by squaring Eq. I13 with a subsequent averaging and keeping terms to second order in the amplitude. Mean values of cross terms i.e. products where the real and imaginary part of the Fourier noise is involved are set to zero.

$$(\frac{d\varphi}{d\omega} - \frac{d\varphi_0}{d\omega})^2 \cong \frac{1}{A_0^2}(\mathrm{Im}(K)\sin(\varphi_0) + \mathrm{Re}(K)\cos(\varphi_0))^2(\frac{d\varphi_0}{d\omega})^2$$
$$+\frac{2}{A_0^2}(\cos(\varphi_0)\frac{d\,\mathrm{Im}(K)}{d\omega} - \sin(\varphi_0)\frac{d\,\mathrm{Re}(K)}{d\omega})(\mathrm{Im}(K)\sin(\varphi_0) + \mathrm{Re}(K)\cos(\varphi_0))\frac{d\varphi_0}{d\omega} \qquad \text{(I15)}$$
$$+\frac{1}{A_0^2}(\cos(\varphi_0)\frac{d\,\mathrm{Im}(K)}{d\omega} - \sin(\varphi_0)\frac{d\,\mathrm{Re}(K)}{d\omega})^2$$

The mean value of Eq. x15 is obtained by using the results in Sec. 1.1 (Eqs. x5, x9).

$$\langle(\frac{d\varphi}{d\omega} - \frac{d\varphi_0}{d\omega})^2\rangle \cong \frac{1}{2A_0^2}(\langle|K|^2\rangle(\frac{d\varphi_0}{d\omega})^2 + \langle\left|\frac{dK}{d\omega}\right|^2\rangle)$$
$$= T^2\frac{E_0\Delta f}{\pi A_0^2}((\frac{1}{T}\frac{d\varphi_0}{d\omega})^2 + \frac{1}{4\pi}\frac{1}{\Delta f T}) \qquad \text{(I16)}$$

Eq. I16 can be rewritten to yield:

$$\langle(\partial t^2\rangle \cong T^2 \frac{1}{\pi\Gamma}((\frac{t_1}{T})^2 + \frac{1}{4\pi}\frac{1}{\Delta fT}) \tag{I17}$$

where $\Gamma = A_0^2 / E_0 \Delta f$ is the square of the signal-to-noise ratio in the Fourier space (∂t and t_1 are introduced in the introduction). The product $E_0 \Delta f$ is the noise energy in the frequency band, and ΔfT is the time-bandwidth product. In the FSI method this last quantity will usual be a large quantity.

The found results can now be used to find the mean and the variance of the impact parameter. The relation between the uncertainty in the impact parameter and the time is given by: $\partial a = (da/dt)\delta t$

By using Eq. x14 we obtain:

$$\langle \partial a \rangle = \frac{da}{dt}\langle \partial t \rangle = 0 \tag{I18}$$

i.e. the measuring of impact parameter is bias free in the FSI method.

The variance of the impact parameter yields:

$$\langle(\partial a^2\rangle = (\frac{da}{dt})^2\langle(\partial t^2\rangle \cong T^2 \frac{1}{\pi\Gamma}\left[(\frac{t_1}{T})^2 + \frac{1}{4\pi}\frac{1}{\Delta fT}\right](\frac{da}{dt})^2 \tag{I19}$$

This is an interesting result, which shows that the uncertainty of the impact parameter increases when the detection time increases. This means that the advantages of having a long synthetic aperture is limited by the thermal noise and that there for a given strength of the noise exist an optimal detection time. The uncertainty in the impact parameter due to the detection time is given by $2\pi/(k\dot{\theta}T)$ where k is the wave number and $\dot{\theta}$ relative angular velocity of the par of satellites.

The effect of the thermal noise propagating in the retrieval chain is, as seen in the previous chapter, a very complex issue. The practical use of the results will mostly be related to Eq. I19 which can be used to find an optimal time aperture in the processing of the occultation signal. In the error analysis of the Abel transform is seen that the errors coming form various sources are affected by the variation of the refractive index and that especially large gradient in the refractive index amplifies the final errors. The effect of these errors can only be described in a statistical framework i.e. in an extensive simulation with 'all' possible refractive index profiles weighted with there the probability of there existence.

References

Born, M. and E. Wolf, Principles of Optics, Cambridge University Press, 1999.

E.T. Goodwin, 'Modern Computing Methods', Notes on Applied Science No. 16, London, Her Majesty's Stationary Office, 1961

Gorbunov M. E., Lauritzen K. B., Analysis of wave fields by Fourier integral operators and their application for radio occultations, *Radio sci.*,39, RS4010, doi:10.1029/2003RS002971, 2004

M. Gorbunov, K. B. Lauritsen, A. Rhodin, M. Tomassini, L. Kornblueh, Analysis of CHAMP radio occultation data for Earth's atmosphere, Izvestiya RAN, Atm. and Ocen.
Phys., submitted, 2005.

Jensen, A. S., Benzon H. H, Lohmann M., A New High Resolution Method for Processing Radio Occultation Data, Scientific Report 02-06, ISSN no. 0905-3263, ISBN no. 87-7478-458-7, *Danish Meteorological Institute*, Copenhagen, 2002a.

Jensen, A. S., Lohmann M., Benzon H.-H., Nielsen A. S., Fourier Analysis of GNSS-LEO Radio Occultation Signals, Resolution and Limitations, *OPAC conf. proc.,* Springer Verlag, *2002b.*

Jensen, A. S., Lohmann M., Benzon H. H., Nielsen A. S, Full Spectrum Inversion of Radio Occultation Signals, *Radio Sci.* 38, (3), 1040, doi: 10.1029/2002RS002763, 2003.

Jensen, A. S. , Lohmann, M. S., Nielsen A. S., Benzon H.-H., Geometrical Optics Phase Matching of Radio Occultation Signals, *Radio Sci.* 39, RS3009, doi: 10.1029/2003RS002899, 2004a.

Previous reports

Previous reports from the Danish Meteorological Institute can be found on:
http://www.dmi.dk/dmi/dmi-publikationer.htm